Available online at www.sciencedirect.com
SCIENCE DIRECT
Journal of Magnetic Resonance 181 (2006) 212–222
JMR Journal of Magnetic Resonance
www.elsevier.com/locate/jmr

Efficiency of paramagnetic relaxation enhancement in off-resonance rotating frame

Huiming Zhang [a,b,*], Yang Xie [a]

[a] Center for Basic MR Research, Evanston Northwestern Healthcare Research Institute, Evanston, IL 60201, USA
[b] Department of Radiology, Feinberg Medical School of Northwestern University, Chicago, IL 60611, USA

Received 2 February 2006; revised 5 May 2006
Available online 2 June 2006

Abstract

Transferring from laboratory frame to off-resonance rotating frame for the ^{1}H spin can compensate the relaxivity loss for paramagnetic agents at the magnetic field strength higher than 3 Tesla and enhance water relaxation rate constant significantly. A comprehensive theory for calculating the relaxation rate constants in the off-resonance rotating frame is described. This theory considers the contributions from both inner shell and outer shell water. The derived relaxation rate constants and relaxation enhancement efficiency as a function of the magnetic field strength and the effective field parameters are directly correlated to the structures, dynamics and environments of paramagnetic agents. To validate the theoretical predictions, we have measured the relaxation enhancement efficiency for a series of macromolecule conjugated gadolinium chelates at 9.4 Tesla. The experimental results confirmed the theoretical predictions. The theory also predicts the relaxation enhancement for T_2-type paramagnetic agents at high magnetic fields. Promising fields of applications include situations where T_1- or T_2-type paramagnetic agents are used for labeling molecular/cellular events.

Keywords: Off-resonance rotating frame; Paramagnetic relaxation enhancement; Gadolinium chelates; Relaxation theory; Molecular dynamics

1. Introduction

Binding paramagnetic chelates to macromolecules can significantly increase the proton spin-lattice relaxation rate of bulky water. This has been a common strategy for improving relaxation efficiency of MRI contrast agents [1,2]. For paramagnetic ions with long electron relaxation time such as Gd(III) or Mn(II), the enhanced relaxivity has a maximum at proton Larmor frequency (ω_H) ~20 MHz. The amplitude of the maximum is a function of the motional correlation time which has been known as proton relaxation enhancement (PRE) since 1970's [3]. However, as the strength of magnet field increases up to $\omega_{S,H}\tau_c \gg 1$, the spectral density function $J(\omega) \to 0$, where ω_S is the electron frequency, $\omega_S = 658\omega_H$, and τ_c is the motional correlation time. τ_c is a function of τ_R, $\tau_c^{-1} = \tau_R^{-1} + \tau_m^{-1} + \tau_s^{-1}$, where τ_s is the electron relaxation time, τ_m is the residence time of structural water, and τ_R is the rotational correlation time. Thus, the relaxivity as a function of spectral density function will decrease rapidly as the magnetic field strength increases. This challenges the application of paramagnetic agents at high magnetic field such as molecular/cellular imaging by MRI, where the concentration of contrast agents may be limited by molecular/cellular events [4].

We have shown recently that transferring from laboratory frame to off-resonance rotating frame for the ^{1}H spin that is dipolar coupled to an electron can alter the frequency dependence of its relaxivity [5]. The off-resonance rotating frame is achieved by a long off-resonance pulse as shown in Fig. 1, which is a routine sequence used in NMR/MRI for spin saturations or magnetization transfer at low offset and RF amplitude [6,7]. The effective field strength (ω_e) of this rotating frame is determined by the RF amplitude of the long pulse (ω_1) and the frequency offset (Δ), $\omega_e = (\omega_1^2 + \Delta^2)^{1/2}$. During the off-resonance pulse, the proton spins of water are aligned to θ angle, $\theta = tg^{-1}(\omega_1/\Delta)$, and relax in the effective field. In order to obtain significant enhancement, a large

* Corresponding author. Fax: +1 847 492 0731.
E-mail address: h-zhang1@northwestern.edu (H. Zhang).

1090-7807/$ - see front matter © 2006 Elsevier Inc. All rights reserved.
doi:10.1016/j.jmr.2006.05.005

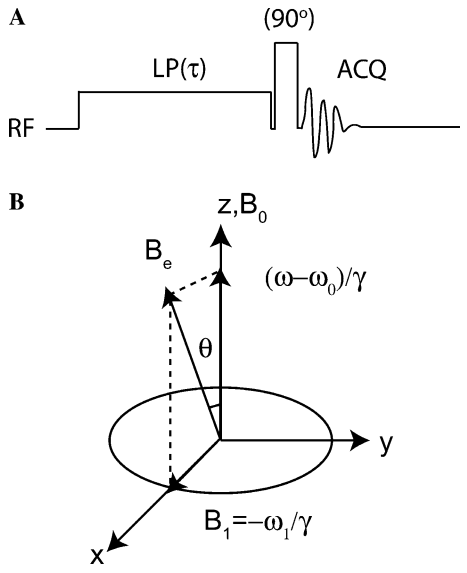

Fig. 1. Off-resonance rotating frame experiment. (A) Pulse sequence. An off-resonance long pulse (LP) of duration τ is applied with RF amplitude ω_1 at frequency offset Δ ($\Delta = \omega - \omega_0$) followed by a 90° pulse on-resonance to detect the residual z-magnetization. (B) Orientation of the off-resonance rotating frame. The off-resonance pulse aligns spins to θ angle, $\theta = \mathrm{tg}^{-1}(\omega_1/\Delta)$, with the effective field of $\omega_e = \sqrt{\omega_1^2 + \Delta^2}$.

θ angle is obtained by using a sufficiently high RF amplitude ω_1 for the off-resonance pulse. The dynamic range of the effective field can be increased significantly by setting the irradiation frequency at offset. At the end of the pulse duration τ, a following 90° pulse reads out the residual z-magnetization. This frame transformation alters the frequency dependence of $J(\omega)$. In the rotating frame, $J(\omega)$ depends primarily on ω_e and partially on ω_H instead of the ω_S and ω_H in the laboratory frame. Since $\omega_e \ll \omega_H$, ω_S, and $\omega_e\tau_c \ll 1$, the effect of the proton relaxation enhancement caused by large $\tau_c(\tau_R)$ will be well preserved. The pulse sequence shown in Fig. 1A is different from another type of rotating frame experiment known as spin-locking [8], where spins are tilted to a θ angle initially followed by an on-resonance spin-locking pulse and a $T_{1\rho}$ time constant is used for describing the loss of magnetization.

In principal, the rotating frame transformation can provide relaxation enhancement in any magnetic field higher than 3 Tesla ($\omega_H = 127$ MHz) if τ_c remains constant. Nevertheless, the τ_s term included in the τ_c expression is magnetic field-dependent. Therefore, analysis of the relaxation rate constant in off-resonance rotating frame as a function of field strength is needed for the purpose of calculating enhanced relaxation rate constants, evaluating enhancement efficiency and extracting structure or dynamic parameters for the paramagnetic labeling.

The motivation of the present work was to establish a correlation between the enhancement efficiency of paramagnetic relaxation and the dynamic parameters of macromolecule conjugated Gd(III) chelates in the off-resonance rotating frame at high magnetic fields. This is only possible if a quantitative theory is available. The primary aim of the present study is to develop such theory.

In this work, we present a comprehensive theory for paramagnetic relaxation enhancement in the off-resonance rotating frame. Starting from the electron-proton dipolar coupling interaction, a complete transformation process from laboratory frame to rotating frame is presented. For simplicity, Bloembergen–Morgan equation is used for calculating τ_s at high magnetic fields [9]. The rotating frame inner shell water relaxation rate constant, like its laboratory frame expression, is derived from the dipolar coupling model. The outer shell water model is an analogous extension of the dipolar coupling interaction in combining with the high field model for Gd(III) chelates developed by Koenig [10,11]. The total rotating frame relaxation rate constant $R_{1\rho}$ combines the inner shell contribution and the outer shell contribution, and is used to define the enhancement efficiency $R_{1\rho}/R_1$. The new features of the rotating frame relaxation rate constants include the spectral density function $J(\omega_e)$ and rotating frame RF parameters. With the theory, numerical calculations were used to simulate the effects of dynamics on $R_{1\rho}$ and $R_{1\rho}/R_1$ as a function of magnetic field or effective field for macromolecule conjugated Gd-DTPA. Experimental data for a series of macromolecule conjugated Gd-DTPA solutions were presented to validate the predictions of the theory.

2. Theory

2.1. Rotating frame spin-lattice relaxation rate constant for electron-proton dipolar coupling

Considering a dipolar coupling of electron spin and proton nucleus under an interaction of RF pulse, the Hamiltonian in the laboratory frame is

$$\tilde{H} = \tilde{H}_z + \tilde{H}_{rf} + \tilde{H}_D, \tag{1}$$

where

$$\tilde{H}_z = \omega_S S + \omega_H I,$$

$$\tilde{H}_{rf} = \omega_1 \exp(-iI_z\omega t) I_z \exp(iI_z\omega t),$$

$$\tilde{H}_D = \sum_{m=-2}^{2} F^{(m)}(t) A^{(m)},$$

$\tilde{H}_z$ is the Zeeman interactions for the electron and the proton nucleus, S and I are the associated electron and proton spin operator. $\tilde{H}_{rf}$ is the RF Hamiltonian. $\tilde{H}_D$ is a second-order tensor for the dipolar coupling between the electron and proton, which can be written as a product sum of spin operators $A^{(m)}$, and time-dependent function of the position coordinates $F^{(m)}(t)$. $A^{(m)}$ and $F^{(m)}(t)$ have properties as follows:

$$A^{(m)} = A^{(-m)\dagger}, \quad F^{(m)}(t) = F^{(-m)^*}(t). \tag{2}$$

The dagger is the Hermitian conjugate and the asterisk denotes the complex conjugate. The spin operators for $m = 0$, 1, 2 are

$$A^{(0)} = S_z I_z - \tfrac{1}{4}(S^+ I^- + S^- I^+),$$

$$A^{(1)} = S_z I^+ + S^+ I_z,$$

$$A^{(2)} = S^+ I^+, \tag{3}$$

where the rising and lowering operators have $S_\pm = S_x \pm iS_y$, $I_\pm = I_x \pm iI_y$. $F^{(m)}(t)$ is a function of second-order spherical harmonics,

$$F^{(0)} = cY_{2,0}(\alpha,\beta) = c(1-3\cos^2\beta),$$
$$F^{(1)} = -\frac{3c}{2}Y_{2,-1}(\alpha,\beta) = -\frac{3c}{2}\sin\beta\cos\beta\exp(-i\alpha),$$
$$F^{(2)} = -\frac{3c}{4}Y_{2,-2}(\alpha,\beta) = -\frac{3c}{4}\sin^2\beta\exp(-2i\alpha), \tag{4}$$

c is coefficient, $c = \gamma_S\gamma_H/r^3$.

To obtain the rotating frame Hamiltonian, a transformation consisting of a series of successive unitary rotations was performed on the laboratory frame Hamiltonian. Since the long pulse is applied on the proton nuclei only, there are three rotations for the proton nuclei and one rotation for the electron spin. The total unitary operator for these rotations is

$$U = U_S U_I = \exp(i\omega_S t S_z)\{\exp(i\omega_e t I_z)\exp(i\theta I_y)\exp(i\omega_H t I_z)\}, \tag{5}$$

where $\theta = tg^{-1}(\omega_1/\Delta), \omega_e = \sqrt{\omega_1^2+\Delta^2}$, as shown in Fig. 1. The Hamiltonian for the rotating frame becomes,

$$\tilde{H}'_D(\omega_e,t) = U\tilde{H}_D U^\dagger, \tag{6}$$

$$\begin{aligned}
\tilde{H}'_D(\omega_e,t) = F^{(0)}\Big\{ & \cos\theta S_z I_z - \frac{\sin\theta}{2}(\exp(i\omega_e t)S_z I^{+\prime} \\
& + \exp(-i\omega_e t)S_z I^{-\prime}) - \frac{1}{4}((\cos\theta-1)/2) \\
& \times [\exp(i(\omega_S-\omega_H-\omega_e)t)S^+I^{+\prime} \\
& + \exp(-i(\omega_S-\omega_H-\omega_e)t)S^-I^{-\prime}] \\
& - \frac{1}{4}\sin\theta[\exp(i(\omega_S-\omega_H)t)S^+I'_z \\
& + \exp(-i(\omega_S-\omega_H)t)S^-I'_z] \\
& - \frac{1}{4}(\cos\theta+1)/2[\exp(i(\omega_S-\omega_H-\omega_e)t)S^+I^{-\prime} \\
& + \exp(-i(\omega_S-\omega_H-\omega_e)t)S^-I^{+\prime}]\Big\} \\
& + F^{(1)}\{(\cos\theta+1)/2[\exp(i(\omega_H+\omega_e)t)S_z I^{+\prime} \\
& + \exp(-i(\omega_H+\omega_e)t)S_z I^{-\prime}] \\
& + \sin\beta[\exp(i\omega_H t)S_z I'_z + \exp(-i\omega_H t)S_z I'_z] \\
& + ((\cos\beta-1)/2)[\exp(i(\omega_H-\omega_e)t)S_z I^{-\prime} \\
& + \exp(-i(\omega_H-\omega_e)t)S_z I^{+\prime}] \\
& - (\sin\theta/2)[\exp(i(\omega_S+\omega_e)t)S^+I^{+\prime} \\
& + \exp(-i(\omega_S-\omega_e)t)S^-I^{-\prime}] \\
& + \cos\theta[\exp(i\omega_S t)S^+I'_z + \exp(-i\omega_S t)S^-I'_z] \\
& - (\sin\theta/2)[\exp(i(\omega_S-\omega_e)t)S^+I^{-\prime} \\
& + \exp(-i(\omega_S-\omega_e)t)S^-I^{+\prime}]\} \\
& + F^{(2)}\{((\cos\theta+1)/2)[\exp(i(\omega_S+\omega_H+\omega_e)t) \\
& \times S^+I^{+\prime}\exp(-i(\omega_S+\omega_H+\omega_e)t)S^-I^{-\prime}] \\
& + (\sin\theta)[\exp(i(\omega_S+\omega_H)t)S^+I'_z \\
& + \exp(-i(\omega_S+\omega_H)t)S^-I'_z] + ((\cos\theta)-1)/2) \\
& \times [\exp(i(\omega_S+\omega_H-\omega_e)t)S^+I^{-\prime} \\
& + \exp(-i(\omega_S+\omega_H-\omega_e)t)S^-I^{+\prime}]\}.
\end{aligned} \tag{7}$$

From the rotating frame Hamiltonian and spin density operator $\sigma(t)$, we can define the motion equation of spin operator, I'_z,

$$\frac{d\langle I'_z\rangle}{dt} = -\frac{1}{2}\sum_m^{\pm2}(J^{(m)}(\omega^{(m)})\mathrm{Tr}\{[A^{(-m)},[A^{(m)},I'_z]](\sigma(t)-\sigma^{eq})\}), \tag{8}$$

where $J^{(m)}(\omega) = \int_{-\infty}^{+\infty} G^{(m)}(\tau)e^{-i\omega t}d\tau$ is the spectra density function, $G^{(m)}(\tau)$ is the correlation function and assuming the motion of the proton spin is random,

$$G^{(m)}(\tau) = \langle F^{(m)}(t)F^{(m)*}(t+\tau)\rangle. \tag{9}$$

Combining Eq. (8) with the following definition,

$$\frac{d\langle I'_z\rangle}{dt} = -R_{1\rho,d}\langle I'_z\rangle - \sigma^{IS}_{\rho,d}\langle S\rangle. \tag{10}$$

We get the rotating frame relaxation rate constant for the electron-proton dipolar coupling,

$$\begin{aligned}
R_{1\rho,d} = K\{ & 2\sin^2\theta J(\omega_e) + \sin^4(\theta/2)J(\omega_S-\omega_H+\omega_e) \\
& + \cos^4(\theta/2)J(\omega_S-\omega_H-\omega_e) \\
& + 3\cos^4(\theta/2)J(\omega_H+\omega_e) + 3\sin^4(\theta/2)J(\omega_H-\omega_e) \\
& + 3/2\sin^2\theta(J(\omega_S+\omega_e)+J(\omega_S-\omega_e)) \\
& + 6\cos^4(\theta/2)J(\omega_S+\omega_H+\omega_e) \\
& + 6\sin^4(\theta/2)J(\omega_S+\omega_H-\omega_e)\}.
\end{aligned} \tag{11}$$

This equation can be simplified as follows by applying the condition $\omega_S \gg \omega_H \gg \omega_e$,

$$R_{1\rho,d} \sim K\{2f_1(\theta)J(\omega_e) + 3f_2(\theta)J(\omega_H)\}. \tag{12}$$

The associated $J^{(m)}(\omega)$ has $\omega = \omega_e, \omega_H$ with $m = 1$, the corresponding spin operators are $S_z I^+$ and its conjugate term $S_z I^-$. In Eqs. (11) and (12),1

$$f_1(\theta) = \sin^2(\theta),$$
$$f_2(\theta) = \sin^4(\theta/2) + \cos^4(\theta/2),$$
$$K = \frac{2}{15}\left(\frac{\mu_0}{4\pi}\right)^2\frac{\hbar^2\gamma_H^2\gamma_S^2 S(S+1)}{r^6},$$
$$J(\omega) = \frac{\tau_c}{1+\omega^2\tau_c^2},$$
$$\tau_c^{-1} = \tau_R^{-1} + \tau_m^{-1} + T_{1e}^{-1},$$
$$T_{1e}^{-1} = \frac{1}{5\tau_{S0}}\left[\frac{1}{1+\omega_S^2\tau_v^2} + \frac{4}{1+4\omega_S^2\tau_v^2}\right],$$

where τ_v is the correlation time characterized the fluctuation of the zero field splitting (ZFS) and τ_{S0} is related to ZFS constant B as $\tau_{S0} = \tau_v/5B$. For the macromolecule conjugated paramagnetic chelates shown in Fig. 2, τ_m is the residual time of structural water, T_{1e} is electronic relaxation time. τ_R is the rotational correlation time, which is a sum of contributions from internal reorientation motion (τ_i) and global tumbling motion (τ_g) and $\tau_R^{-1} = \tau_i^{-1} + \tau_g^{-1}$.

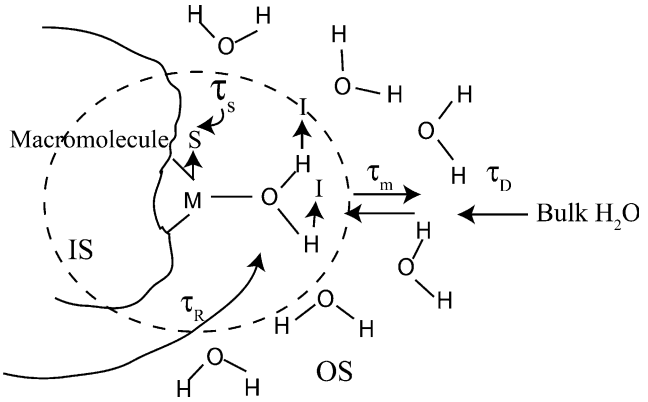

Fig. 2. A schematic of the spin relaxations in the solution of macromolecule conjugated paramagnetic chelates. The coordinated water is directly bound to the metal ion and forms the inner shell (IS), its relaxation rate constant is determined by three dynamic parameters, namely the electron relaxation time τ_s or T_{1e}, the residence time of coordinated water τ_m and the rotational correlation time of the paramagnetic unit τ_R. Other surrounding water forms the outer shell (OS), the relaxation rate constant is determined by the diffusion correlation time τ_D.

2.2. Rotating frame spin-lattice relaxation rate constant for inner sphere water

The inner shell water relaxation results from a chemical exchange of water molecules involving the primary coordination sphere of the paramagnetic metal ion. In the laboratory frame, the relaxation rate constant R_1^{IS} is as follows [3]:

$$R_1^{IS} = \frac{P_m q}{1/R_{1,d} + \tau_m}, \tag{13}$$

where P_m is the molar fraction of metal ion, q is the number of water molecular bound per metal ion. $R_{1,d}$ is the relaxation rate constant of the bound water, τ_m is the residual life time of the bound water. In the off-resonance rotating frame, $R_{1,d}$ is replaced by $R_{1\rho,d}$. Assuming $1/R_{1,d}$, $1/R_{1\rho,d} \gg \tau_m$, this will lead to $R_{1\rho}^{IS} = P_m q R_{1\rho,d}$ and $R_1^{IS} = P_m q R_{1,d}$.Thus, we obtain the relationships as follows:

$$R_{1\rho}^{IS}/R_1^{IS} = R_{1\rho,d}/R_{1,d}, \tag{14}$$

$$R_{1\rho}^{IS}/R_1^{IS} = \frac{2}{3} K f_1(\theta)(1 + (\omega_H \tau_c)^2) + f_2(\theta). \tag{15}$$

The rotating frame relaxation rate constant $R_{1\rho}^{IS}$ is a function of the hydration water number q and their mole fraction P_m. But, the enhancement efficiency $R_{1\rho}^{IS}/R_1^{IS}$ shown in Eq. (14) is irrelevant to q and P_m for the inner shell water alone. Eq. (15) shows that the enhancement efficiency will increase as the square of the motional correlation time τ_c and the magnetic field strength ω_H.

2.3. Rotating frame spin-lattice relaxation rate constant for outer shell water

For the spin relaxation of Gd(III) chelates in the laboratory frame, Koenig, etc. has developed an outer sphere model [10,11], which fits well with the experimental data obtained from high magnetic fields for gadolinium chelates and iron oxide nanoparticles. The relaxation rate constant R_1^{OS} is expressed as

$$\begin{aligned} R_1^{OS} = K'\{&7[1 - (\alpha B_S^2(x)/2) J_{2OS}(\omega_S, \tau_D, T_{2e})] \\ &+ 3[(1+\alpha) B_S^2(x) J_{1OS}(\omega_H, \tau_D, T_{1e} \to \infty) \\ &+ (1 - B_S^2(x)) J_{1OS}(\omega_H, \tau_D, T_{1e})]\}, \end{aligned} \tag{16}$$

where

$$K' = \frac{32\pi}{405}\hbar^2\gamma_H^2\gamma_S^2 S(S+1)\frac{N_A}{1000}\left(\frac{C}{dD}\right),$$

$$B_S(x) = \left(\frac{2S+1}{2S}\right)\coth\left[\left(\frac{2S+1}{2S}\right)x\right] - \left(\frac{1}{2S}\right)\coth\left[\frac{x}{2S}\right],$$

$$\begin{aligned} J_{nOS}(\omega_H, \tau_D, T_{ne}) = \mathrm{Re}\{&1 + (1/4)(i\omega\tau_D + \tau_D/T_{ne})\} \\ &/\{1 + (i\omega\tau_D + \tau_D/T_{ne})^{1/2} + (4/9)(i\omega\tau_D \\ &+ \tau_D/T_{ne}) + (1/9)(i\omega\tau_D + \tau_D/T_{ne})^{3/2}\}, \end{aligned}$$

where $x = \mu B_0/RT$, $\alpha = (2S-1)/(S+1)$ and $\tau_D = d^2/D$. D is the sum of the diffusion coefficients of water molecule (D_I) and metal ion complex (D_S), d is the distance of closest approach of the water molecule to the metal complex, μ is the magnetic moment of the metal ion, $\mu = \gamma_S \hbar S$.

In the similar way discussed above for the electron-proton dipolar coupling interaction, the relaxation rate constant is transferred to the off-resonance rotating frame. Assuming $\omega_S \gg \omega_H \gg \omega_e$, the relaxation rate constant $R_{1\rho}^{OS}$ in the rotating frame is as follows:

$$\begin{aligned} R_{1\rho}^{OS} = K'\{&2f_1(\theta)(1 + \alpha B_S^2(x)) J_{1OS}(\omega_e) \\ &+ 3f_2(\theta)[(1+\alpha) B_S^2(x) J_{1OS}(\omega_H, \tau_D, T_{1e} \to \infty) \\ &+ (1 - B_S^2(x)) J_{1OS}(\omega_H, \tau_D, T_{1e})]\}. \end{aligned} \tag{17}$$

The outer shell relaxation rate constant has a similar expression as the inner shell except that the spectral density function is more complicated. Nevertheless, we can use numerical calculation to simulate the influence of related factors, as discussed later. Eq. (17) is also suitable for T_2-type paramagnetic agents, where the major contribution to the relaxation is from the outer shell water [10].

2.4. Total relaxation rate constant in off-resonance rotating frame

The total relaxation rate constant in off-resonance rotating frame $R_{1\rho}$ is the contribution sum of the inner shell water and outer shell water,

$$R_{1\rho} = R_{1\rho}^{IS} + s R_{1\rho}^{OS}, \tag{18}$$

where s is the space assessable coefficient for the outer shell water for macromolecule conjugated paramagnetic ions and $0.5 < s < 1.0$. Since $R_{1\rho}^{IS}$ and $R_{1\rho}^{OS}$ depend on θ angle, $R_{1\rho}$ is also a function of θ, $R_1 < R_{1\rho} < R_2$ for $0 < \theta < 90°$.

2.5. Relaxation enhancement efficiency

Experimental measurement for the relaxation enhancement efficiency can be measured with the pulse sequence

shown in Fig. 1A, where the long off-resonance pulse with duration τ tilts proton spins to θ angle as defined in Fig. 1B. The 90° pulse reads out the residual z-magnetization. When spin arrives at equilibrium with the rotating frame, the residual z-magnetization is defined as follows [12]:

$$M_e(\tau \to \infty) = M_0 \cos^2\theta \frac{R_1}{R_{1\rho}}. \quad (19)$$

The $\cos^2\theta$ term in Eq. (19) accounts for the direct saturation effect of RF irradiation.

The measured relaxation rate constants normally are sum of the paramagnetic contribution from metal ions and the diamagnetic contribution from the solvent and the conjugated macromolecules, as shown below,

$$(R_{1,1\rho})_{\text{measured}} = (R_{1,1\rho})_{\text{diamag}} + (R_{1,1\rho})_{\text{paramag}}. \quad (20)$$

If $(R_{1,1\rho})_{\text{diamag}} \ll (R_{1,1\rho})_{\text{paramag}}$, then the enhancement efficiency can be determined directly from the measured residual magnetization using the following equation,

$$\frac{R_{1\rho}}{R_1} = \frac{M_0}{M_e(\infty)} \frac{1}{\cos^2\theta}. \quad (21)$$

Another factor to influence the measurement of $R_{1\rho}/R_1$ is the magnetization transfer effect [7]. For macromolecule conjugated paramagnetic agents in aqueous solutions, this effect can be neglected since the concentration of the macromolecule can be lower than 0.1 mM.

2.6. Numerical simulations

Calculations of relaxation rate constants and enhancement efficiencies were performed for macromolecule conjugated Gd-DTPA. The parameters used in the calculations are $S = 7/2$, $q = 1$–3, $\tau_{s0} = 85$ ps, $\tau_v = 38$ ps, $\tau_m = 0.244$ μs, $r = 3.05$ Å, $\tau_R = 80$, 500, 1000, 1500, 2000 and 3000 ps, $d = 3.6$ Å, $D = 3.16 \times 10^{-5}$, 1.0×10^{-5}, 8.0×10^{-6}, 5.0×10^{-6}, 2.0×10^{-6}, 1.0×10^{-6} cm^2/s, $s = 0.75$. For simulated $R_{1\rho}/R_1$ as a function of frequency offset, RF amplitude is 2, 4 and 6 kHz, and offset Δ varies from 5 to 60 kHz. All calculations were carried out with the mathematical software Mathematica.

3. Experimental

3.1. Synthesis of paramagnetic agents

Bovine serum albumin (BSA, Mw 68 kDa) from Aldrich was dissolved in 0.1 M Hepes buffer at pH 7.4, a 200-fold excess dianhydride c-DTPA was added in five equal portions during 1 h at room temperature [13]. The solution was stirred for 1 h and then passed through a 0.2 μm filter. In an ice bath, equal mole of $GdCl_3$ to DTPA was added into the filtrate in five equal portions during 1 h at pH 6.0. The solution was stirred for 24 h at 4 °C, and Arsenazo III was used to test free Gd^{3+} ion [14]. The solution was centrifuged with Amicon Ultra-15 from Millipore with molecular weight cutoff (MWCO) of 5 kDa, and lyophilized to a white solid powder. The product was analyzed for protein concentration by UV absorbency at 595 nm with Bradford assay and for gadolinium content by atomic emission spectroscopy (AES). A molecular formula of $(Gd\text{-}DTPA)_{30}$-BSA was found for this product.

Polylysine (PLS, Mw 15–30 kDa) from Aldrich was dissolved in 0.1 M sodium bicarbonate buffer at pH 9.0, a 40-fold excess dianhydride c-DTPA was added in five equal portions during 1 h at ice bath [13]. This mixture was warmed up to room temperature and stirred for 6 h. A small portion of the resulting solution containing PLS-DTPA was purified for structure analysis. A colorimetric assay was used to determine the binding percentage of DTPA. The remaining portion was reacted with $GdCl_3$ for 6 h and Arsenazo III was used to test free Gd^{3+} ion. The solution was centrifuged with Amicon Ultra-15 from Millipore (Billerica, MA) with molecular weight cutoff (MWCO) of 5 kDa and lyophilized to a white solid powder. The averaged molecular formula of the contrast agent is $(Gd\text{-}DTPA)_{32}$-PLS.

Dextran (Mw 15–20 kDa) from Fluka, dried overnight at 70 °C, was reacted with DTPA dianhydride at a ratio of 1 DTPA per 2 glucose units in dry DMSO at 60 °C for 30 min [15]. After adding water and adjusting pH to 6, $GdCl_3$ based on 1:1 mole ratio to DTPA was added and allowed to react for 5 h. Free Gd^{3+} test was negative with Arsenzo III. The resulting solution was ultra-filtrated by Amicon Ultra-15 and lyophilized. The mole ratio of DTPA to Dextran was determined by elemental analysis. The averaged molecular formula of the contrast agent was found to be $(Gd\text{-}DTPA)_8$-Dextran.

One percent of PAMAM dendrimer-g_5 (Mw 28.8 kDa) from Sigma–Aldrich was mixed with 45-fold excess p-SCN-benzyl-DTPA (Macrocyclics, Hoston, TX) [16]. The mixed solution was adjusted to pH 9 and maintained at 40 °C for 24 h. $GdCl_3$ was added into the solution and stirred for 5–6 h. Free Gd^{3+} test was negative with Arsenzo III. The resulting solution was ultra-filtrated by Amicon Ultra-15 and lyophilized. The mole ratio of DTPA to PAMAM was determined by elemental analysis. The molecular formula of the contrast agent is $(Gd\text{-}DTPA\text{-}SCN\text{-}Bz)_{41}$-PAMAM-g5.

3.2. NMR measurements

All NMR experiments were carried with volume coils on a 9.4 T Bruker Advance micro-imaging spectrometer. Samples at 1 mM gadolinium concentration were placed in a 5 mm tube in a Bruker ^{1}H 10 mm resonator at room temperature. The off-resonance rotating frame magnetization profiles were obtained by applying a long pulse with a 5–60 kHz frequency offset followed by a 90° reading pulse. Residual magnetization was plotted as a function of offset frequency to generate the magnetization profiles. The applied long off-resonance pulses were 500 ms long with RF amplitudes of 2, 4 and 6 kHz.

4. Results and discussions

4.1. Inner shell water contribution

Fig. 3 shows the laboratory frame relaxation rate constant R_1^{IS}, the off-resonance rotating frame relaxation rate constant $R_{1\rho}^{IS}$, and the enhancement efficiency, $R_{1\rho}^{IS}/R_1^{IS}$, for the inner shell water at $\omega_H = 10$–1000 MHz and $\theta = 50°$. These calculated rate constants only include the paramagnetic contribution. For chelates with one structural water molecule, $q = 1$, as the rotational correlation time τ_R increases from 80 to 3000 ps, R_1^{IS} has a maximum at frequency ~20 MHz and decreases rapidly as the frequency increases. However, the profile for $R_{1\rho}^{IS}$ is different, it shows a nearly constant dependence on the frequency. The amplitude of $R_{1\rho}^{IS}$ is much higher than R_1^{IS} and is proportional to the rotational correlation time τ_R. The influence of τ_R is via the expression of τ_c, $\tau_c^{-1} = \tau_R^{-1} + \tau_m^{-1} + T_{1e}^{-1}$. In this calculation, τ_m is 0.244 ms, T_{1e} is around 2.2 ns at 20 MHz and increases rapidly as the square of the frequency. τ_R begins to dominate the motion correlation time τ_c at ~50 MHz and equals to τ_c at higher field due to $\tau_R \ll \tau_m, T_{1e}$. As the result, $R_{1\rho}^{IS}$ increases as τ_R increases. Fig. 3 is calculated by using Eqs. (12) and (15) based on the electron-proton dipolar coupling, which may represent a simplified model for Gd-DTPA. Gd^{3+} ion is known to have static and transient zero field splitting (ZFS) effect at low magnetic fields, which can generate multiple transitions for its electron relaxation [17–19]. Since most Gd(III) complexes have the ZFS in the order of 0.1 cm^{-1} (~0.3 Tesla), their electron relaxation should be located in the Zeeman limit ($H_{Zeeman} \gg H_{ZFS}$) at the magnetic field strength higher than 3 Tesla [20]. Thus, the complication due to non-degenerate electron states may be not a problem for the evaluation of electron relaxation time. In additions, τ_c is determined by τ_R at high field. However, the effect of the transient ZFS on the proton spin relaxation needs to be explored further, which is out the scope of this paper.

From R_1^{IS} and $R_{1\rho}^{IS}$, the enhancement efficiency $R_{1\rho}^{IS}/R_1^{IS}$ are calculated as a function of the square of τ_R and ω_H, which increases rapidly as the magnetic field strength and the rotational correlation time increase. As shown in Fig. 3, $R_{1\rho}^{IS}/R_1^{IS}$ ranges from 1.1 to 140 at $\omega_H = 1000$ MHz for paramagnetic agents with τ_R of 80–3000 ps. Notice that for a given τ_R, the higher enhancement efficiency, $R_{1\rho}^{IS}/R_1^{IS}$, does not necessarily correspond to a larger $R_{1\rho}^{IS}$, i.e., $R_{1\rho}^{IS}$ at 1000 MHz is lower than $R_{1\rho}^{IS}$ at 100 MHz. $R_{1\rho}^{IS}/R_1^{IS}$ defines the dynamic range for magnetizations of rotating frame. But for different τ_R, higher enhancement efficiency always corresponds to the larger relaxation rate constant $R_{1\rho}^{IS}$. In this case, $R_{1\rho}^{IS}$ or $R_{1\rho}^{IS}/R_1^{IS}$ can be used to differentiate the dynamics of the paramagnetic agents, as we will discuss in a successive paper.

4.2. Outer shell water contribution

Fig. 4 plots the laboratory frame relaxation rate constant R_1^{OS}, the off-resonance rotating frame relaxation rate constant $R_{1\rho}^{OS}$ and the enhancement efficiency $R_{1\rho}^{OS}/R_1^{OS}$ of outer shell water at $\omega_H = 10$–1000 MHz and $\theta = 50°$. These calculated rate constants only include the paramagnetic contribution to water relaxation. In this calculation, τ_R is 80 ps, which corresponds to that for the small paramagnetic complex Gd-DTPA. The water diffusion constant is varied from 3.16×10^{-5} cm^2/s that of pure water at 37 °C to 1×10^{-6} cm^2/s for slow "local diffusion" expected of tissue

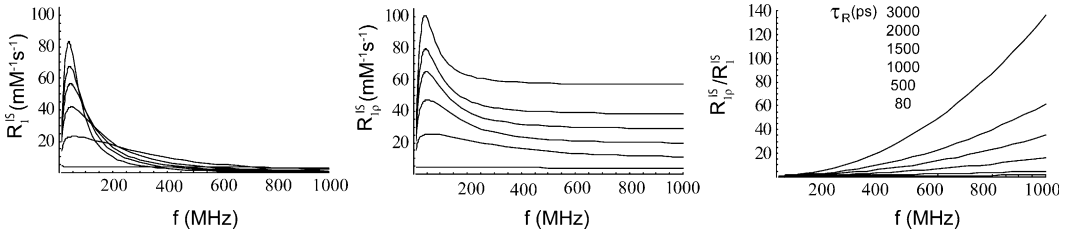

Fig. 3. Theoretically predicted relaxation rate constants and enhancement efficiency for the inner shell water as a function of proton Larmor frequency for macromolecular conjugated Gd-DTPA. The profiles are corresponding to the rotational correlation time τ_R of 80–3000 ps. Molecular parameters are discussed in the text.

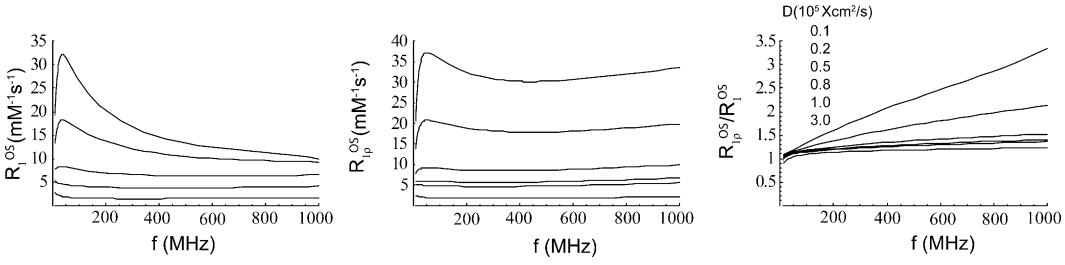

Fig. 4. Theoretically predicted relaxation rate constants and enhancement efficiency for the outer shell water as a function of proton Larmor frequency for Gd-DTPA. The profiles are for the diffusion coefficient D ranged from 3.1×10^{-5} to 1×10^{-6} cm^2/s. Molecular parameters are discussed in the text.

water vide infra. Since the effective distance for the electron-nuclear dipolar interaction is limited to a few nm [21], the diffusion constant used here is the parameter that characterizes water motion within the immediate local vicinity of the paramagnetic relaxation center. We note that the MR determined apparent diffusion constant (ADC) of for exercised fixed tissue water has been reported to be as low as 10^{-7} cm^2/s [22,23]. However, the ADC reflects the presence of numerous mesoscopic scale hindrances and restrictions to water displacement imposed by the complex microstructure of tissue. Thus, the MR determined tissue water ADC does not provide a measure of the local diffusion coefficient that is associated with the spectral density function of the outer shell water. The local diffusion coefficient can be associated with the barrier-free viscosity of the aqueous cellular milieu. The local water diffusion coefficient (sometimes referred to as the free diffusion coefficient) or the corresponding media viscosity has been inferred from a variety of studies employing small molecules or ions as reporter species. Derived water diffusion coefficient values ranging from 1×10^{-5} cm^2/s in cells to 1×10^{-6} cm^2/s in 4% agarose gels [24–28] are typical. In the laboratory frame, R_1^{OS} has a maximum and appears at frequency ~20 MHz only if the diffusion coefficient is sufficiently low, i.e., $D<5\times10^{-6}$ cm^2/s. As the field strength increases, R_1^{OS} decreases rapidly. This is attributed to the behavior of the spectral density functions, J_{2OS} (ω_S, τ_D, T_{2e}) and J_{1OS} (ω_H, τ_D, T_{1e}). τ_D will become very large for a small diffusion coefficient, $\tau_D=d^2/D$ and make the $\omega_{S,H}\tau_D$ term dominant in $i\omega_{S,H}\tau_D+\tau_D/T_{ne}$. In the rotating frame, since the primary frequency dependence is the effective field ω_e, the $\omega_e\,\tau_D$ term becomes a small number that is insufficient to dominate $i\omega_e\tau_D+\tau_D/T_{1e}$. The relaxation rate constant $R_{1\rho}^{OS}$ is nearly constant, increasing gradually as the frequency moves above 300 MHz. It is always greater than the corresponding R_1^{OS}. The rotating frame enhancement contribution mainly comes from the J_{1OS} (ω_e) term. This term will significantly affect $R_{1\rho}^{OS}$ in the presence of a small local diffusion coefficient, because the relaxation rate constant K' in Eq. (17) is proportional to $1/D$. On the other hand, τ_D is determined by the distance d between the paramagnetic center and the surrounding "associated water" (i.e., by the dimension of the particle). For an iron oxide nanoparticles, d equals to the radius of the nanoparticles. In this case, τ_D characterizes the time scale required for water to diffuse away from the influence of nanoparticles, τ_D increases as the size of the nanoparticles increases [10]. K' will be reduced because it is proportional to d as well. Nevertheless, the relaxivity loss due to large τ_D can be regained by the off-resonance rotating frame method. Most T_2-type paramagnetic agents, such as iron oxides nanoparticles, have large τ_D values, their T_1 relaxivity has a maximum at 10–20 MHz and decreases as the magnetic field increases [10,29]. Thus, the method described in the paper can be used to enhance the rotating frame relaxation rate constants $R_{1\rho}$ for the T_2-type agents at high magnetic fields. The detection of the T_2-type agents by the rotating frame weighted imaging will generate hyperintense contrast instead the hypointense contrast obtained in the conventional T_2-weighted imaging, as shown in our recent report for MIONs at 9.4 Tesla [30].

4.3. Total relaxation rate constants in off-resonance rotating frame

Fig. 5 shows the total laboratory frame relaxation rate constant R_1, the total off-resonance rotating frame relaxation rate constant$R_{1\rho}$, and the enhancement efficiency $R_{1\rho}/R_1$, at $\omega_H=10$–1000 MHz and $\theta=50°$. These calculated rate constants only include the paramagnetic contribution. Fig. 5A is for Gd-DTPA with diffusion coefficient $D=3.16\times10^{-5}$ cm^2/s, hydration number $q=1$ and $\tau_R=80$–3000 ps. R_1 and $R_{1\rho}$ are slightly higher than those for the inner shell model shown in Fig. 3, since the contribution from the outer shell water is much smaller than that from the inner shell water for most τ_R at this diffusion coefficient. But the enhancement efficiency $R_{1\rho}/R_1$ is much lower than that for the inner shell, especially for very large τ_R at high magnetic field. For τ_R of 3000 ps at 1000 MHz, $R_{1\rho}/R_1$ is 40 in comparing with 140 for the inner shell water alone. Although the $R_{1\rho}/R_1$ for both cases increases as the frequency increases, the increment becomes smaller for the full shell water starting from $\omega_H\sim600$ MHz. This simply arises from that $R_1^{OS}>R_1^{IS}$ for large τ_R at $\omega_H>600$ MHz, consequently, R_1^{OS} dominates R_1 and limits the enhancement efficiency $R_{1\rho}/R_1$.

Alteration of the structure or the dynamic environment of paramagnetic agents can substantially change the enhancement efficiency, since q is related to the structure of the paramagnetic chelate, τ_R is related to the dynamics of the paramagnetic chelate and D is related to the local environment of the paramagnetic chelate. As an example, if the hydration number q increases, the inner shell water will dominate the total relaxation rate constant. Fig. 5B shows the same calculation as Fig. 5A except for the hydration number $q=3$. In this case, both R_1 and $R_{1\rho}$are tripled but not the enhancement efficiency. It is 70 for τ_R of 3000 ps at $\omega_H=1000$ MHz instead 40 for $q=1$. On the other hand, if the outer shell relaxation rate constant increases due to the decrease of diffusion coefficient, both R_1 and $R_{1\rho}$ will become substantially larger than that of the inner shell water, as shown in Fig. 5C for $D=1.0\times10^{-6}$ cm^2/s. As the result, their ratio $R_{1\rho}/R_1$ will become smaller, i.e., ~10 for τ_R of 3000 ps at 1000 MHz, and the increment of $R_{1\rho}/R_1$ slows down beginning at lower frequency such as 400 MHz. Thus, quantitative information about the dynamics for the paramagnetic agent as labeling probe can be extracted from the relaxation enhancement effect in the off-resonance rotating frame.

4.4. Effect of θ angle

All the calculations presented above are performed at a single θ angle ($\theta=50°$) and expressed in proton Larmor

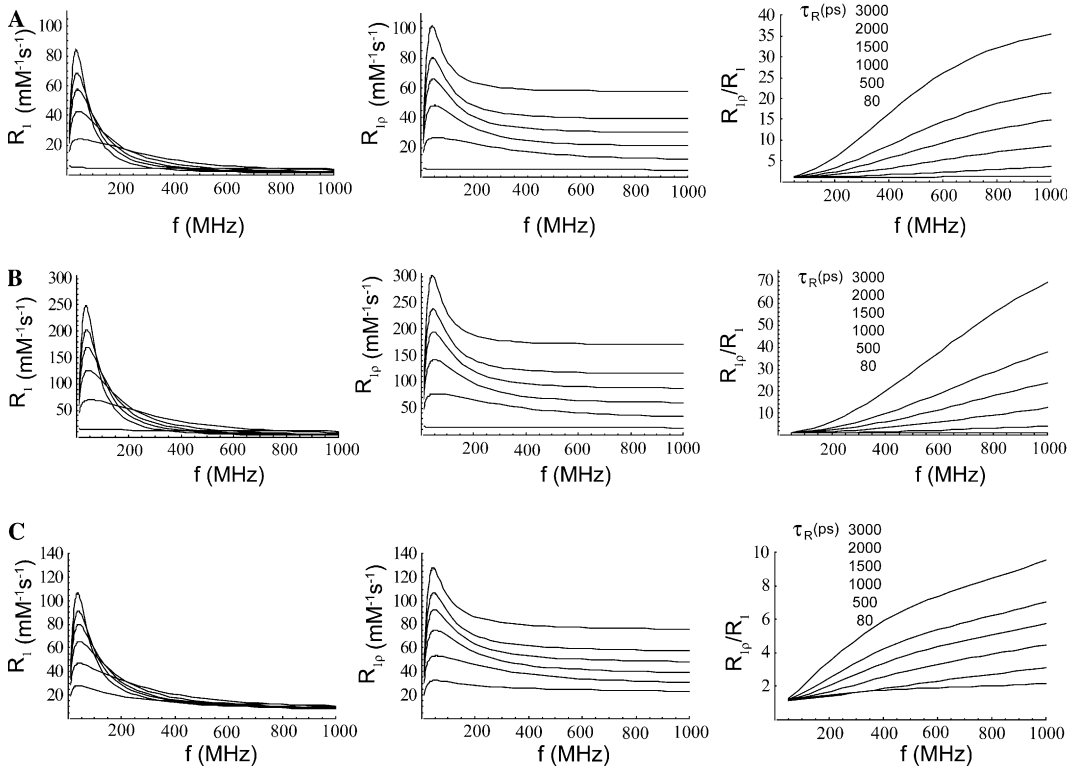

Fig. 5. Theoretically predicted relaxation rate constants and enhancement efficiency for the sum of the inner shell water and the outer shell water as a function of proton Larmor frequency. The profiles were calculated for macromolecular conjugated Gd-DTPA of different structures or dynamic environment. The rotational correlation time τ_R ranges from 80 to 3000 ps and the space assessable coefficient s for the outer shell water is 0.75. (A) Single coordinated water $q = 1$ and fast diffusion coefficient $D = 3.16 \times 10^{-5}$ cm^2/s. (B) Three coordinated water $q = 3$ and fast diffusion coefficient $D = 3.16 \times 10^{-5}$ cm^2/s. (C) Single coordinated water $q = 1$ and slow diffusion coefficient $D = 1.0 \times 10^{-6}$ cm^2/s. Molecular parameters are discussed in the text.

frequency frame. For general consideration, the effect of θ angle on the enhancement efficiency $R_{1\rho}/R_1$ can be expressed in the off-resonance rotating frame as a function of frequency offset (Δ) at given RF amplitude (ω_1). Fig. 6 shows the θ angle, $f_1(\theta)$ and $f_2(\theta)$ as a function of frequency offset at three RF amplitudes $\omega_1 = 2$, 4 and 6 kHz. A larger θ angle can be obtained with a larger RF amplitude at a smaller frequency offset, i.e., $\omega_1 = 6$ kHz and $\Delta = 5$ kHz yield $\theta = 50°$, $\omega_1 = 2$ kHz and $\Delta = 5$ kHz result $\theta = 22°$. $f_1(\theta)$ and $f_2(\theta)$ actually are θ-dependent coefficient functions, $f_1(\theta)$ determines the contribution from $J(\omega_e)$ and $f_2(\theta)$ determines the contribution from $J(\omega_H)$. Fig. 6 shows that $f_1(\theta)$ increases with the increase of θ angle at $\Delta < 30$ kHz and $\omega_1 < 6$ kHz; while $f_2(\theta)$ decrease with the increase of θ angle at $\Delta < 20$ kHz. This defines the relaxation enhancement in the region of $\Delta < 30$ kHz.

4.5. Calculated enhancement efficiency

$f_1(\theta)$ and $f_2(\theta)$ determine the distribution of enhancement efficiency $R_{1\rho}/R_1$ in the off-resonance rotating frame. Fig. 7 shows $R_{1\rho}/R_1$ as a function of Δ with $\omega_1 = 2$,4 and 6 kHz at 9.4 Tesla ($\omega_H = 400$ MHz). For Gd-DTPA at 25 °C, $D = 3.16 \times 10^{-5}$ cm^2/s and $\tau_R = 500$, 750 and 1250 ps, the maximum enhancement efficiency ranges from 1.6 up to 4.3 at $\omega_1 = 6$ kHz and $\Delta = 5$ kHz. For $\tau_R = 500$ or 750 ps at this field strength, the hydration number q does not affect the $R_{1\rho}/R_1$ too much. Therefore, $R_{1\rho}/R_1$ for $q = 2$ is slightly higher than that for $q = 1$. But for $\tau_R = 1250$ ps, the influence is much stronger. Fig. 7 also provides information for estimating the τ_R for the experimental $R_{1\rho}/R_1$ shown below. The largest frequency offset for a detectable $R_{1\rho}/R_1$ is proportional to the square of ω_1 and τ_R, which

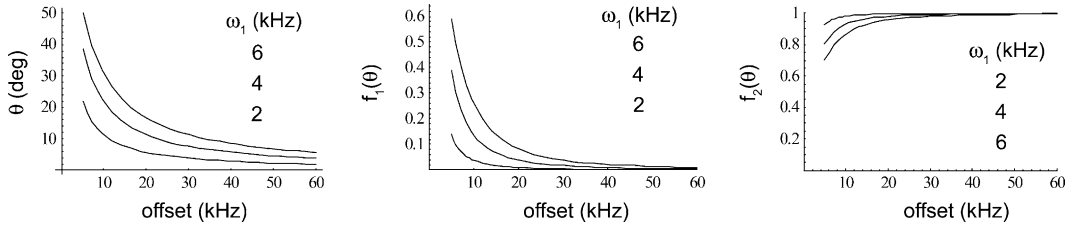

Fig. 6. Effect of effective field θ angle. θ angle, $f_1(\theta)$ and $f_2(\theta)$ as a function of frequency offset at RF amplitude of 2, 4 and 6 kHz.

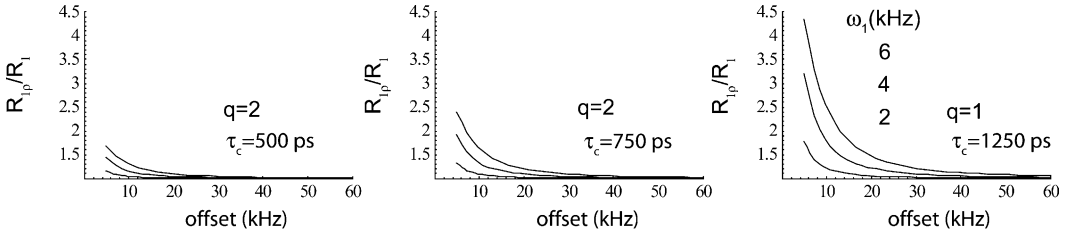

Fig. 7. Theoretically predicted relaxation enhancement efficiency $R_{1\rho}/R_1$ as a function of frequency offset at RF amplitude of 2, 4 and 6 kHz. Three macromolecule conjugated Gd-DTPA with $\tau_R = 500$, 750 and 1250 ps and $D = 3.16 \times 10^{-5}$ cm^2/s were calculated for magnetic field strength of 9.4 Tesla.

varies between 15 and 35 kHz. There is a broad dynamic range for detecting the relaxation enhancement for paramagnetic agents with large τ_R, which will be further extended by using a higher strength of magnetic field. This feature permits one to select RF parameters in wide range so that the enhancement is detected at low RF amplitude within the limit of the specific absorption rate (SAR). Thus the paramagnetic relaxation enhancement will benefit from high B_0 in term of the sensitivity and dynamic range for detection, which will be potentially important for biological applications if SAR can be reduced [31].

4.6. Experimental enhancement efficiency

Fig. 8 shows the experimental enhancement efficiency for the aqueous solutions of $(Gd\text{-}DTPA)_8$-Dextran, $(Gd\text{-}DTPA)_{31}$-PLS, $(Gd\text{-}DTPA)_{30}$-BSA and $(Gd\text{-}DTPA\text{-}SCN\text{-}Bz)_{41}$-PAMAM-g5 at 1 mM Gd concentration. The concentration of these macromolecules ranges from 0.125 to 0.025 mM. The magnetization transfer effect due to their slow tumbling motions can be neglected. Since the T_1 is shorter than 200 ms for these solutions and is longer than 2 s for the solvent, the diamagnetic contribution from the solvent can be neglected from their relaxation rate constants. Thus, the measured magnetization can be directly used to calculate the enhancement efficiency. The Dextran, PLS, BSA conjugated DTPA were synthesized by reacting the macromolecules with c-DTPA, their hydration number q is 2. The PAMAM-g5 conjugated DTPA was synthesized by reacting the macromolecules with the SCN-Bz-DTPA. Its conjugation functional group SCN-Bz is directly attached to the backbone of the DTPA, which leaves eight dentates to coordinate with Gd(III) and one structural site for the water molecule ($q = 1$). In these macromolecules, both polylysine and Dextran are linear polymers and very flexible. The excess-OH group in Dextran can facilitate the water exchange. BSA is a globular shape protein and is less flexible than the linear polymers. PAMAM-g5 is the most rigid macromolecule among these macromolecules and has a spherical shape. From these structural information, the order of molecular dynamics for these macromolecules is Dextran $\sim$ polylysine $>$ BSA $>$ PAMAM-g5, where the more rigid molecule has the less local mobility. The measured enhancement efficiency for

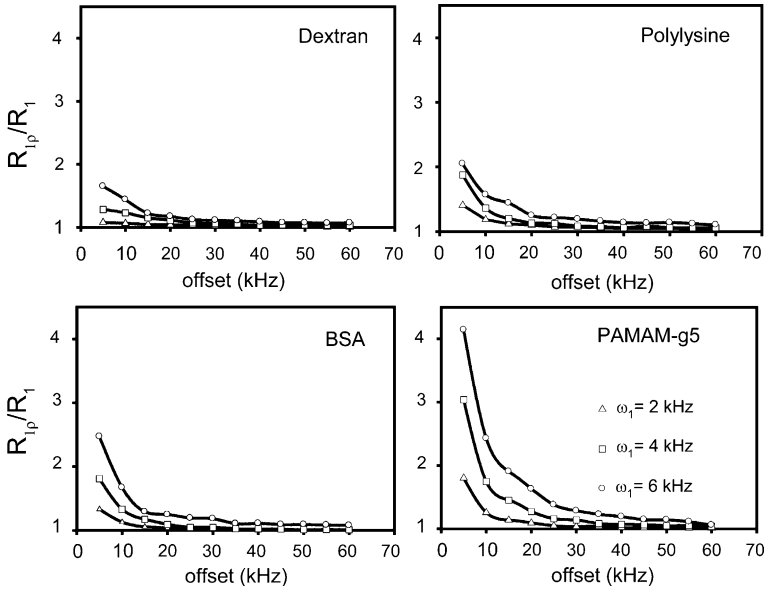

Fig. 8. Experimentally measured relaxation enhancement efficiency $R_{1\rho}/R_1$ as a function of frequency offset at RF amplitude of 2, 4 and 6 kHz. Four macromolecule conjugated Gd-DTPA at 1 mM Gd(III) were examined at magnetic field strength of 9.4 Tesla. Their averaged molecular formula are $(Gd\text{-}DTPA)_8$-Dextran, $(Gd\text{-}DTPA)_{31}$–PLS, $(Gd\text{-}DTPA)_{30}$-BSA and $(Gd\text{-}DTPA\text{-}SCN\text{-}Bz)_{41}$-PAMAM-g5.

these macromolecule conjugated Gd-DTPA is in the order of PAMAM-g5 > BSA > PLS > Dextran. Explicitly, the $R_{1\rho}/R_1$ value at $\omega_1 = 6$ kHz and $\Delta = 5$ kHz is 4.3 for PAMAM-g5, 2.5 for BSA, 2.2 for polylysine and 1.7 for Dextran.

This measurement not only provides the enhancement efficiency but also the dynamics of the paramagnetic unit for each macromolecule. By comparing Figs. 7 and 8, the effective motional correlation can be estimated as PAMAM-g5 $\sim$ 1.3 ns, BSA $\sim$ 0.75 ns, PLS $\sim$ 0.65 ns, dextran $\sim$ 0.5 ns. Although the molecular weight of these macromolecule conjugated is in the order of $(Gd\text{-}DTPA)_{30}$-BSA($\sim$85 kDa) > $(Gd\text{-}DTPA\text{-}SCN\text{-}Bz)_{41}$-PAMAM-g5 ($\sim$60 kDa) > $(Gd\text{-}DTPA)_{31}$–PLS (30 kDa $\sim$ 45 kDa) > $(Gd\text{-}DTPA)_8$-Dextran (20–25 kDa), apparently, the internal reorientation motion plays important role in the overall rotation correlation time due to $\tau_R^{-1} = \tau_i^{-1} + \tau_g^{-1}$. Thus, reducing the internal rotational correlation time can effectively increase the relaxation rate constant in the off-resonance rotating frame.

5. Conclusions

A comprehensive relaxation theory in the off-resonance rotating frame for water molecules in presence of paramagnetic agents has been developed. According to the theory, the relaxation rate constants in the off-resonance rotating frame can be substantially increased in comparison with their laboratory frame values. The enhancement efficiency is directly related to the structures, dynamics and environments of the paramagnetic agents themselves, in addition to the magnetic field strength and the effective field parameters. Thus, the dynamics of paramagnetic agents can be extracted from the measurement of water NMR signals, which contain parameters such as rotation correlation time, water hydration number and diffusion coefficient, as shown in the examples of Gd(III) chelates at high magnetic field ($B_0 > 3$T). The experimental data for a series of macromolecule conjugated Gd-DTPA confirmed the predictions of the theory. The relaxation enhancement method discussed in this work is effective for the inner shell water and the outer shell water, thus, is capable to raise the relaxation efficiency for those T_1-type and T_2-type paramagnetic relaxation agents that are used for labeling molecular/cellular events. The essence of this approach is to capture a low frequency spectral density function $J(\omega_e)$ to enhance the paramagnetic relaxation rate constant even through the experiment is performed at high magnetic fields. The $J(0)$ in the transverse relaxation rate constant R_2 contains the similar information as the $J(\omega_e)$, but the sensitivity for detecting the paramagnetic agents of large R_2 is low at high fields, i.e., the images for these agents normally appear to be hypointense. The $T_{1\rho}$ method presented in this paper permits to enhance the relaxivity and provide high detection sensitivity simultaneously.

Acknowledgment

This work was supported by grant to H.Z. from the National Institutes of Health (EB02912).

References

[1] R.B. Lauffer, Paramagnetic metal complexes as water proton relaxation agents for NMR imaging: theory and design, Chem. Rev. 87 (1987) 901–927.
[2] P. Caravan, J.J. Ellison, T.J. McMurry, R.B. Lauffer, Gadolinium(III) chelates as MRI contrast agents: structure, dynamics, and applications, Chem. Rev. 99 (1999) 2293–2352.
[3] D.R. Bruton, S. Forsen, G. Karlstrom, Proton relaxation enhancement (PRE) in biochemistry: a critical survey, Progress in NMR spectroscopy 13 (1979) 1–45.
[4] R. Weissleder, U. Mahmood, Molecular imaging, Radiology 219 (2001) 316–333.
[5] H. Zhang, L.H. Bryant, A.M. Wyrwicz, Paramagnetic enhancement in off-resonance rotating frame, Proc. Int. Soc. Magn. Reson. 7 (1999) 340.
[6] P.J. Keller, W.W. Hunter Jr, P. Schmalbrock, Multisection fat-water imaging with chemical shift selective presaturation, Radiology 164 (1987) 539–541.
[7] S.D. Wolff, R.S. Balaban, Magnetization transfer contrast (MTC) and tissue water proton relaxation in vivo, Magn. Reson. Med. 10 (1989) 135–144.
[8] S.R. Charagundla, A. Borthakur, J.S. Leigh, R. Reddy, Artifacts in T(1rho)-weighted imaging: correction with a self-compensating spin-locking pulse, J. Magn. Reson. 162 (2003) 113–121.
[9] N. Bloembergen, L.M. Morgan, Proton relaxation times in paramagnetic resolutions. Effects of spin relaxation, J. Chem. Phys. 34 (1961) 842–850.
[10] S.H. Koenig, K.E. Kellar, Theory of 1/T1 and 1/T2 NMRD profiles of solutions of magnetic nanoparticles, Magn. Reson. Med. 34 (1995) 227–233.
[11] K.E. Kellar, P.M. Henrichs, M. Spiller, S.H. Koenig, Relaxation of solvent proton by solute Gd^{3+}-chelates revisited, Magn. Reson. Med. 37 (1997) 730–735.
[12] T. Schleich, C.F. Morgan, G.H. Caines, Protein rotational correlation times by carbon-13 rotating-frame spin-lattice relaxation in presence of off-resonance radiofrequency field, Methods Enzymol. 176 (1989) 386–418.
[13] P.F. Sieving, A.D. Watson, S.M. Rockage, Preparation and characterization of paramagnetic polychelates and their protein conjugates, Bioconjug. Chem. 1 (1990) 65–71.
[14] L.H. Bryant Jr, M.W. Brechbiel, C. Wu, J.W.M. Bulte, V. Herynek, J.A. Frank, Synthesis and relaxometry of high-generation (G = 5,7,9, and 10) PAMAM dendrimer-DOTA-gadolinium chelates, J. Magn. Reson. Imaging 9 (1999) 348–352.
[15] F.E. Armitage, D.E. Richardson, K.C.P. Li, Polymeric contrast agents for magnetic resonance imaging: synthesis and characterization of gadolinium diethylenetriaminepentaacetic acid conjugated to polysaccharides, Bioconjug. Chem. 1 (1990) 365–374.
[16] E.C. Wiener, M.W. Brechbiel, H. Brothers, R.L. Magin, O.A. Gansow, D.A. Tomalia, P.C. Lauterbur, Dendrimer-based metal chelates: a new class of magnetic resonance imaging contrast agents, Magn. Reson. Med. 31 (1994) 1–8.
[17] P.H. Fries, C. Gateau, M. Mazzanti, Practical routine to relative diffusion coefficients and electronic relaxation rates of paramagnetic metal complexes in solution by model-independent outer-sphere NMRD. Potentiality for MRI contrast agents, J. Am. Chem. Soc. 127 (2005) 15801–15814.
[18] A. Borel, F. Yerly, L. Helm, A.E. Merbach, Multiexponential electronic spin relaxation and Redfield's limit in Gd(III) complexes in solution: consequences for $^{17}O/^1H$ NMR and EPR simultaneous analysis, J. Am. Chem. Soc. 124 (2002) 2042–2048.

[19] X. Zhou, P. Caravan, R.B. Clarkson, P.-O. Westlund, On the philosophy of optimizing contrast agents. An analysis of ^{1}H NMRD profiles and ESR lineshapes of the Gd(III) complex MS-325 +HAS, J. Magn. Reson. 167 (2004) 47–160.

[20] R.B. Clarkson, A.I. Smirnov, T.I. Smirnova, H. Kang, R.L. Belford, J.H. Freed, Multi-frequency EPR determination of zero field splitting of high spin species in liquids: Gd(III) chelates in water, Mol. Phys. 95 (1998) 1325–1332.

[21] J. Jacob, B. Baker, R.G. Bryant, D.S. Cafiso, Distance estimates from paramagnetic enhancements of nuclear relaxation in linear and flexible model peptides, Biophys. J. 77 (1999) 1086–1092.

[22] D.L. Buckley, J.D. Bui, M.I. Philips, T. Zelles, B.A. Inglis, H.D. Plant, S.J. Blackband, The effect of ouabain on water diffusion in the rat hippocampal slice measured by high resolution NMR imaging, Magn. Reson. Med. 41 (1999) 137–142.

[23] T.M. Shepherd, E.D. Wirth III, P.E. Thelwall, H.X. Chen, S.N. Roper, S.J. Blackband, Water diffusion measurements in perfused human hippocampal slices undergoing Tonicity changes, Magn. Reson. Med. 49 (2003) 856–863.

[24] J.V. Sehy, J.J.H. Ackerman, J.J. Neil, Apparent diffusion of water, ions, and small molecules in the xenopus oocyte is consistent with brownie displacement, Magn. Reson. Med. 48 (2002) 42–51.

[25] C.D. Kroenke, J.J.H. Ackerman, D.A. Yablonskiy, On the Nature of the NAA diffusion attenuated MR signal in the central nervous system, Magn. Reson. Med. 52 (2004) 1052–1059.

[26] B.J. Balcom, T.J. Lees, A.R. Sharp, N.S. Kulkarni, G.S. Wagner, Diffusion in Fe(II/III) radiation dosimetry gels measured by magnetic resonance imaging, Phys. Med. Biol. 40 (1995) 1665–1676.

[27] T.V. Pedersen, D.R. Olsen, A. Skretting, Measurement of the ferric diffusion coefficient in agarose and gelatine gels by utilization of the evolution of radiation induced edge as reflected in relaxation rate images, Phys. Med. Biol. 42 (1997) 1575–1585.

[28] M.W. Hodges, D.S. Cafiso, C.F. Polnaszek, C.C. Lester, R.G. Bryant, Water translational motion at the bilayer interface: an NMR relaxation dispersion measurement, Biophys. J. 73 (1997) 2575–2579.

[29] J.W. Bulte, R.A. Brooks, B.M. Moskowitz, L.H. Bryant, J.A. Frank, T_1 and T_2 relaxometry of monocrystalline iron oxide nanoparticles (MION-46L): theory and experiment, Acad. Radiol. 5 (1998) S137–S140.

[30] H. Zhang, A.M. Wyrwicz, Paramagnetic relaxation enhancement in off-resonance rotating frame: from Gd-DTPA to MIONs, Proc. Int. Soc. Magn. Reson. 8 (2000) 2061.

[31] R.R. Regatte, S.V.S. Akella, A.J. Wheaton, A. Borthakur, J.B. Kneeland, R. Reddy, $T_{1\rho}$-relaxation mapping of human femoral-tibial cartilage in vivo, J. Magn. Reson. Imaging 18 (2003) 336–341.